Thesis for the Degree of Licentiate of Engineering

1060 nm GaAs VCSELs for Extended Reach Optical Interconnects in Data Centers

Ewa Simpanen

Photonics Laboratory
Department of Microtechnology and Nanoscience (MC2)
Chalmers University of Technology
Göteborg, Sweden 2018

1060 nm GaAs VCSELs for Extended Reach Optical Interconnects in Data Centers

Ewa Simpanen

Technical report no MC2-389
ISSN 1652-0769

Photonics Laboratory
Department of Microtechnology and Nanoscience (MC2)
Chalmers University of Technology
SE-412 96 Göteborg
Sweden
Telephone: +46 (0) 31 772 1000

Printed by Chalmers reproservice, Chalmers University of Technology
Göteborg, Sweden 2018

1060 nm GaAs VCSELs for Extended Reach Optical Interconnects in Data Centers

Ewa Simpanen

Photonics Laboratory
Department of Microtechnology and Nanoscience (MC2)
Chalmers University of Technology

Abstract

The data centers of today are increasing in size and are built to accommodate strong data traffic demands while providing sustainably by having clients sharing resources under one roof. Their massive scale puts pressure on the server network topology and has incited a need for data transmission links that are energy efficient and capable to operate at high bit rates with reach up to a few kilometers. Optical interconnects (OIs) offer large bandwidth and low attenuation at long distances, and are therefore suitable for this task. The most commonly used OIs, with 850 nm GaAs-based vertical-cavity surface-emitting lasers (VCSELs) and multi-mode fiber (MMF), have a 25 Gb/s reach that is limited to a few hundred meters. However, the fiber chromatic dispersion and attenuation that limit the OI reach can be reduced significantly by increasing the wavelength of this very same technology. The upper limit of the GaAs-based VCSEL technology, with strained InGaAs quantum wells (QWs), is about 1100 nm.

With further improved OI performance, new hyperscale data center topologies can be realized and explored. This will lead to many more possible solutions in traffic engineering as well as for power management. 1060 nm VCSELs could open up for lane rates of 10, 25 and possibly 50 Gb/s over distances up to 2 km and help reach the Tb/s link speed aim of the Ethernet standard.

In this work we show that the 1060 nm GaAs VCSEL is a suitable light source for long-reach OIs by demonstrating its overall stable performance and capability of error-free data transmission up to 50 Gb/s back-to-back and 25 Gb/s over 1 km of MMF. These results stem from careful VCSEL design, including strained InGaAs QWs with GaAsP barriers, doped AlGaAs distributed Bragg reflectors, a short optical cavity and multiple oxide layers. We also show that the fabrication of such a device poses no increase in complexity and can be realized using standard processing techniques.

Keywords: vertical-cavity surface-emitting laser, optical interconnect, chromatic dispersion, attenuation, reach, high-speed modulation, single-mode, multi-mode

List of Papers

This thesis is based on the following appended papers:

[A] **E. Simpanen**, J. S. Gustavsson, E. Haglund, E. P. Haglund, A. Larsson, W. V. Sorin, S. Mathai, and M. R. Tan, "1060 nm single-mode vertical-cavity surface-emitting laser operating at 50 Gbit/s data rate," *Electronics Letters*, vol. 53, no. 13, pp. 869-871, June 2017.

[B] A. Larsson, **E. Simpanen**, J. S. Gustavsson, E. Haglund, E. P. Haglund, T. Lengyel, P. A. Andrekson, W. V. Sorin, S. Mathai, M. R. Tan, and S. R. Bickham, "1060 nm VCSELs for long-reach optical interconnects," *Optical Fiber Technol. (2018)*, https://doi.org/10.1016/j.yofte.2018.01.001.

Related conference publications and presentations by the author:

[C] **E. Simpanen**, J. S. Gustavsson, E. Haglund, E. P. Haglund, A. Larsson, W. V. Sorin, S. Mathai, and M. R. Tan, "1060 nm VCSEL for up to 40 Gbit/s data transmission," *2016 International Semiconductor Laser Conference (ISLC)*, Sept. 2016.

[D] **E. Simpanen**, J. S. Gustavsson, E. Haglund, E. P. Haglund, T. Lengyel, A. Larsson, P. A. Andrekson, W. V. Sorin, S. Mathai, M. R. Tan, and S. Bickham, "1060 nm single and multimode VCSELs for up to 50 Gb/s modulation," *2017 IEEE Photonics Conference (IPC)*, pp. 65-66, Oct. 2017.

Acknowledgement

A thank you to all of you who have supported me in this work.

I would like to thank my supervisor and examiner Prof. Anders Larsson for his contagious interest and curiosity in photonics, and for always looking onward to the future. Thanks to my co-supervisor Johan Gustavsson who shares his knowledge in VCSELs with patience and care. Petter Westbergh taught me how great VCSELs are made and Erik and Emanuel Haglund have always been there for support, in fabrication, characterization and matters big and small - thank you.

I am lucky to have such fantastic colleagues at Photonics Laboratory you are all dear to me. Special thanks to Mikael Mazur, Lars Lundberg, TamÃąs Legyel, Sheila Galt and Jörgen Bengtsson for keeping me on track. Without the support of IT and administration at MC2 I would not be able to get work done. I would also like to thank the staff of the Nanofabrication Laboratory who always keep the machines at best performance and generously share their knowledge.

Thanks to our collaborators Mike Tan, Wayne Sorin, and Sagi Mathai at Hewlett Packard Enterprise in Palo Alto and Scott Bickham at Corning for insightful discussions and contribution to my work.

The research on 1060 nm VCSELs was financially supported by Hewlett Packard Enterprise Innovation Research Program and the Swedish Foundation for Strategic Research (SSF). 1060 nm optimized MMF was designed and manufactured by Corning. IQE Europe is acknowledged for supplying the epitaxial VCSEL material.

My final gratifications are dedicated to Jenny and Mathias.

Ewa Simpanen

Göteborg
March 2018

List of Abbreviations

BCB benzocyclobutene
BR bit rate
BW bandwidth
DBR distributed Bragg reflector
DMT discrete multitone
DSP digital signal processing
EEL edge-emitting laser
FEC forward error correction
HPC high-performance computing
ICP inductively-coupled plasma
MM multi-mode
MMF multi-mode fiber
MOCVD metal-organic chemical vapor deposition
MQW multiple quantum wells
OI optical interconnect
OOK on-off keying
PAM-4 four-level pulse amplitude modulation
PECVD plasma-enhanced chemical vapor deposition
QW quantum well
RIE reactive ion etching
RTP rapid thermal processor
SM single-mode
SMF single-mode fiber
TLM transfer length method (or transmission line model)
ToR Top of Rack
VCSEL vertical-cavity surface-emitting laser

Table of Contents

Chapter 1

Introduction

Data centers are a base component of Internet infrastructure used for storage, computation and access to data. The simplest data center is a small server room and further advanced is a high-performance computing (HPC) system. This last decade the digital economy has been accommodated by quickly building more and more data centers, many privately owned and maintained. This has led to excessive redundancy in the network, with underutilization of servers and low energy efficiency. With an approximate lifespan of 5 years, many data centers are already operating with outdated technology that is in need of update and puts high demand on maintenance, causing neglect and costly downtime [1–3]. The massive global traffic consumption and the development of cloud computing now move workload away from small, privately managed, data centers and increase the demand for larger data centers [1, 2, 4–6]. These data centers are often referred to as mega, warehouse, exascale or hyperscale data centers and at the end of 2015 there were 259 located around the world, hosting 21% of all data center servers, 39% of all processing power, 49% of all stored data and 34% of all traffic recorded from all data centers [7].

The number of hyperscale data centers is planned to grow to 485 by 2020 [7], seen in Figure 1.1. The environmental impact caused by data centers due to energy consumption and emission of green house gases has risen a large public interest in green cooling and power [1–4], and the incentive to optimize utilization and cut energy costs is high for mega data center operators [1, 2, 8]. Many projects are therefore employing new network topologies, virtualization, traffic engineering, power management and renewable energy access as ways to improve energy efficiency and develop into green data centers [1–4, 8]. The

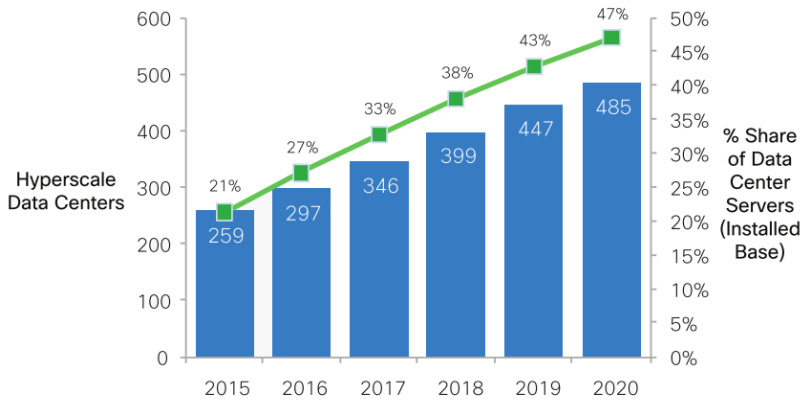

Figure 1.1: Hyperscale data center growth from 2015 to 2020 [7].

aim is to decrease power consumption, increase utilization and control thermal behavior [1] and fiber optics is a key enabler to advance data center technology towards this goal [3].

1.1 Architecture of a Hyperscale Data Center

Hundreds of thousands of servers form the basis of a hyperscale data center. The servers are stacked in racks of about 40 to 80 units, in which they are interconnected via a Top of Rack (ToR) switch. The ToRs are then connected using additional layers of network switches. A hyperscale data center demands careful consideration when building the topology of the switch network. In addition to network throughput, latency, congestion and packet loss [1, 3], the upscaled topology also needs to support a large inter-node communication bandwidth (BW), so that applications can exchange information with remote nodes when needed to then be able to proceed with their local computation. For this purpose, topologies such as the fat-tree was proposed [9], illustrated in Figure 1.2, and it is designed to spread outgoing traffic from any given instance as evenly as possible among the core switches. The fat-tree topology has been well received to be used in large data centers due to its large bisectional BW, economical scalability and backward compatibility [3–5, 8, 9], as well as its fault tolerance and energy efficiency, with low power consumption and heat dissipation compared to a typical, strongly hierarchical design [3]. However, as server performance is improved and the data centers grow larger, the scalability of this topology becomes limited by the many interconnections. Thus, there

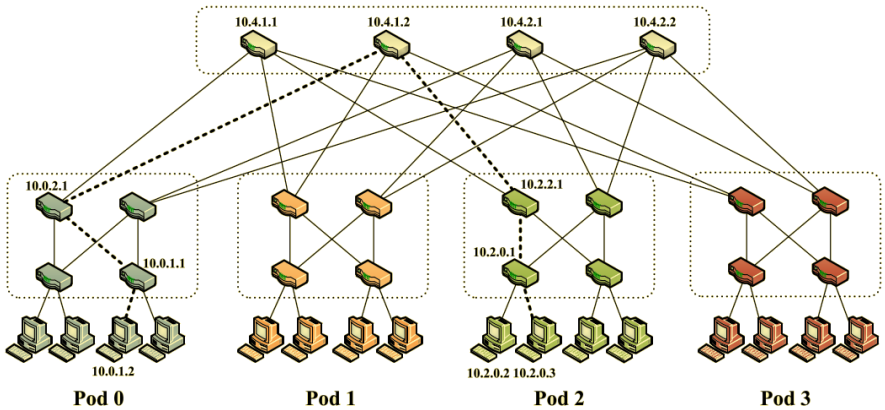

Figure 1.2: In this simplified view of the fat-tree topology, packets from source 10.0.1.2 to destination 10.2.0.3 take the dashed path [9]. The core layer of switches is on top and it communicates via an aggregation layer of switches to reach any edge switch.

is an intense need for interconnects operating at higher bit rates (BRs) and longer reach.

Compared to electrical transmission, a fiber-optic cable can provide high data rates with large BW, there is little attenuation and since there is no crosstalk or any electromagnetic interference [10, 11], fibers can easily be bundled. The optical interconnect (OI) for data center application is further described in Chapter 2. The most common OI uses 850 nm vertical-cavity surface-emitting laser (VCSEL)s with multi-mode fiber (MMF) [5]. Commercialized 850 nm OIs can provide 25 Gb/s lane rate up to at least 100 m [12], but if the reach was to exceed this limit they would suffer greatly from fiber chromatic dispersion and attenuation. Hyperscale data centers require a minimum fiber reach of about 500 m [13], and up to 2 km [12]. With limited reach, the 850 nm VCSEL and MMF OIs have been pinpointed a significant bottleneck [6, 14]. However, by extending the wavelength of the GaAs-based VCSEL it is possible to drastically reduce the effects of chromatic dispersion and attenuation in the MMF and meet the requirement for longer reach. The purpose of this work is to investigate the potential of increasing the operating wavelength of the standard OI, and demonstrate a 1060 nm VCSEL as a light source for high modulation speeds over longer distances.

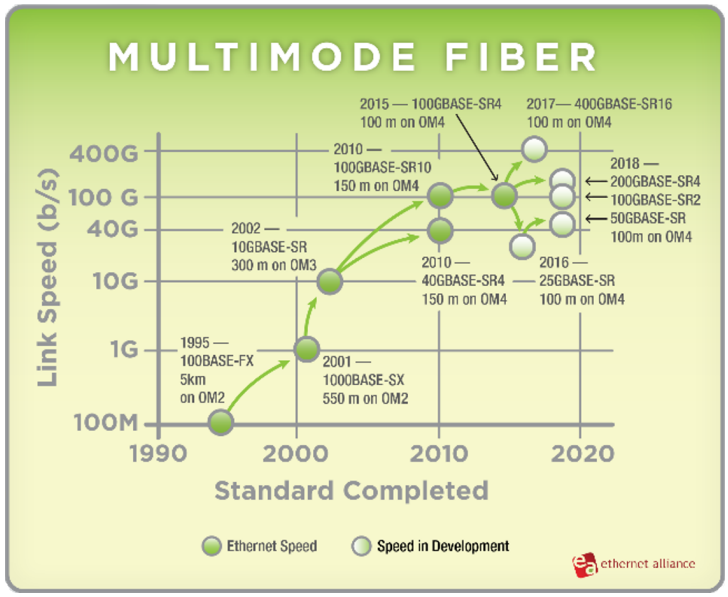

Figure 1.3: MMF Ethernet Roadmap 2016 [15].

1.2 The Ethernet Standard and Future Prospects

Ethernet is a standard for short reach communication and it governs local area networks, based on electrical and optical links. The electrical standards are typically used for interconnects shorter than 5 m, the optical MMF standards are employed for links longer than 5 m, and the single-mode fiber (SMF) standards for 500 m and above [12]. Using binary modulation, single lane optical link speeds range from 10 Gb/s to 100 Gb/s, and with higher order modulation 200 Gb/s single lane rate is realized. The Ethernet Roadmap for MMF, in Figure 1.3, shows that 10 Gb/s lanes are integrated to form the 40GBASE-SR4 and 100GBASE-SR10 standards that reach 150 m, while parallel 25 Gb/s lanes build up to 400 Gb/s aggregate capacity using 16 fiber pairs of 100 m length [15]. Future link speeds, aiming beyond 400 Gb/s, will be in the Tb/s range. A possible standard, following up on highly parallel speeds with 100 Gb/s lanes, is 1.6 Tb/s [12, 16].

Since transmission distance in MMF becomes limited at higher data rates, multiple parallel links are aggregated. With 1060 nm VCSELs, lane rates of 10, 25 and 50 Gb/s over distances up to 2 km are of interest and could serve to develop the Ethernet standard.

Chapter 2

Optical Interconnect Technologies

The OI transmits and receives data in the optical domain and provides an electrical interface that can connect to electrical equipment such as switches in a data center. The typical VCSEL-based OI transmitter consists of a driver and a VCSEL, as in Figure 2.1a, and the receiver of a photodetector and an amplifier, in Figure 2.1b. The driver directly modulates the VCSEL and the output is passed on to an optical fiber, which is then received by the detector and converted back to an electrical signal that is amplified to sufficient levels.

The optical communication channel provides broad BW transmission, with low but wavelength dependent attenuation (2 dB/km at 850 nm, 1 dB/km at 1060 nm, 0.2 dB/km at 1550 nm) [17], immunity to electromagnetic interfer-

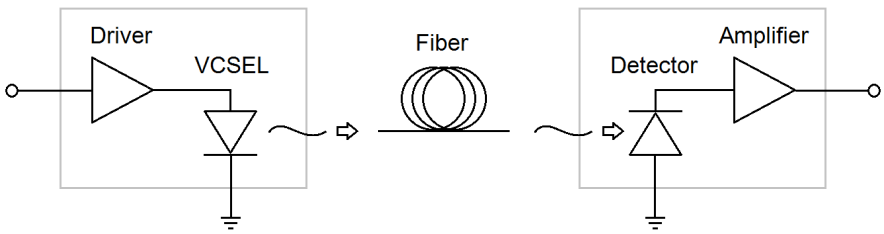

Figure 2.1: The optical channel of a VCSEL-based OI. Input data is applied to the driver that modulates the VCSEL and the resulting optical signal is coupled to the fiber. On the receiver end, a photodetector converts the optical signal back to electrical and the data is then amplified and passed along.

ence, electrical insulation, and security of information [18]. The fiber is also light weight, has a low material cost and a lower risk of theft than copper. Basic fiber transmission principles are discussed in Section 2.1.

OIs enable the high parallelism used in the Ethernet standard. Data centers require bundable cables and transmission with low energy consumption and good thermal properties [1]. As covered in Chapter 1, the interconnects in hyperscale data centers also need to transmit at high BR over distances up to 2 km [12]. In this type of facilities, small size and low cost transceivers are highly desirable. MMF is more expensive per unit length but better fiber coupling properties makes them more cost efficient and thus heavily used in data centers [19].

The VCSEL, introduced in Section 2.2, is often considered the ideal light source for OIs, mainly because of its circular output and possibility for high speed modulation. VCSELs are low-cost devices that can be directly modulated, have high power efficiency and better allow for fabrication in volume and test-on-wafer. However, it is important to design the VCSEL for high reliability and temperature stability.

Despite the limited reach of 850 nm MMF OIs, the 850 nm VCSEL dominates the market for transmitters used in fiber optic data communication links [20]. It is the most commonly used wavelength in Ethernet, Fibre Channel and Infiniband standards. The reasons are the high performance, high efficiency and low cost of the well-established VCSEL technology at this wavelength. High-speed MMF is also available at 850 nm and polymer waveguide loss is lower than at longer wavelengths [21]. SMF can be used to extend reach but it requires single-mode (SM) lasers, more critical alignment and therefore increased cost. Another way is to use many parallel links as in the Ethernet standard in Section 1.2, but this is limited by rack space and the size of pluggable transceivers. The preferred choice would be to increase distance and throughput in a single fiber, with no need for duplicate hardware in several links and reduced overall complexity.

At longer wavelengths, fiber performance improves. The VCSEL emission wavelength depends on the semiconductor material system it is based upon. 850 nm VCSELs are GaAs-based. $Al_xGa_{1-x}As$ compounds are used in the mirrors and the gain wavelength can be extended to about 1.1 µm using $In_xGa_{1-x}As$ quantum wells (QWs) [22]. 1310 nm and 1550 nm VCSELs based on InP compounds suffer from higher current densities for sufficient gain due to high levels of non-radiative recombination in the active region materials [23]. A small refractive index contrast also makes it more difficult to design mirrors with high enough reflectivity at these wavelengths.

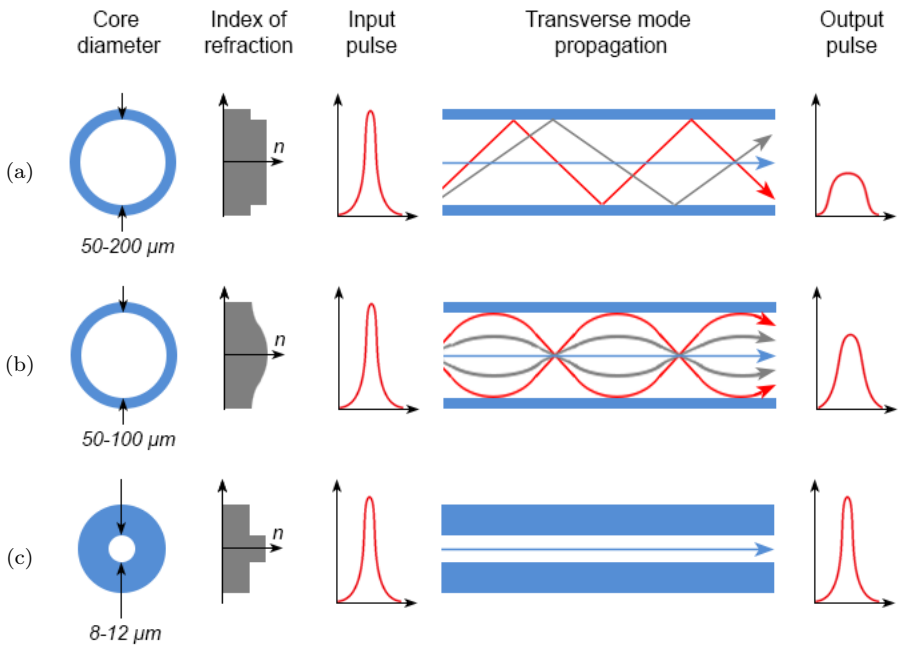

Figure 2.2: Core size, refractive index profile, mode propagation and temporal input/output of a) step-index MMF, b) graded-index MMF, and c) SMF.

2.1 Optical Fibers

Many of the advantageous properties of OIs are established by the optical fiber. Optical fibers are often drawn from silica, which is a low cost and light-weight material that has good transmission over a wide range of wavelengths, low losses due to absorption and scattering, and high resistance to both mechanical and optical damage. The structure of the fiber can be very simple, with a single core having a higher refractive index than its surrounding cladding, relying on total internal reflection to guide light along its length. [24]

With large enough core diameter and refractive index step, the fiber supports several transverse modes, which is illustrated in Figure 2.2a. A MMF supports many propagation paths, but at longer distance the impact of modal dispersion becomes significant. By introducing a graded index core, as in Figure 2.2b, light will instead follow sinusoidal paths down the fiber which helps reduce modal dispersion. The larger core of the MMF makes connections easier and increases alignment tolerance. In Figure 2.2c, it is shown that SMF only supports propagation of the fundamental mode due to its relatively small core

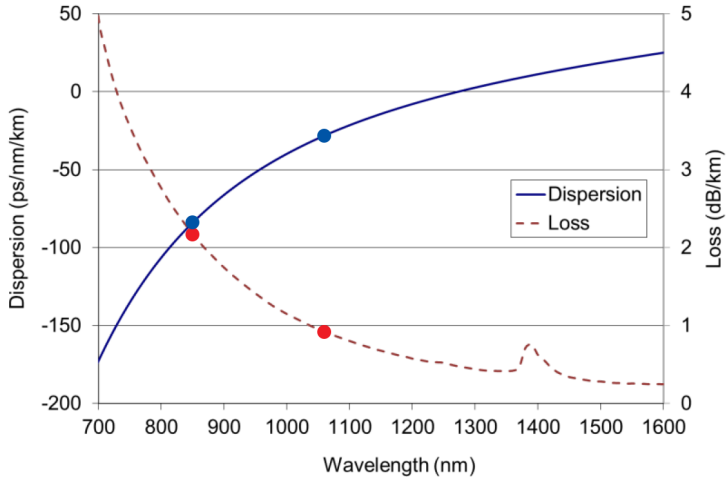

Figure 2.3: MMF chromatic dispersion and attenuation versus wavelength [26].

size. SMF is exempt from intermodal dispersion and can carry transmission over even longer distances. [24]

Chromatic dispersion and attenuation also limit the reach of fiber transmission and are currently the main constraints of 850 nm OIs [6, 14]. Increasing the operating wavelength reduces these effects. However, the wavelength is restricted by the light source of the OI, and the GaAs technology limits the VCSEL wavelength to about 1.1 µm [22]. MMF has less than half of the attenuation and only a third of the chromatic dispersion at 1060 nm compared to 850 nm [25], as seen in Figure 2.3.

2.2 Oxide-Confined GaAs VCSELs

The VCSEL is a semiconductor laser in which the cavity and the propagation of photons is oriented vertically to the plane of the layers that provide optical gain, as shown in Figure 2.4a. Due to this geometry, the VCSEL has transverse symmetry and a circularly shaped optical beam. In contrast to an edge-emitting laser (EEL), seen in Figure 2.4b, the reversed dimensions of the VCSEL, with the short cavity and less restricted lateral size, separates the longitudinal modes and may increase the number of transverse modes. Differently sized VCSELs can be designed with more flexibility. A larger device aperture will result in a more powerful multi-mode (MM) VCSEL with a more

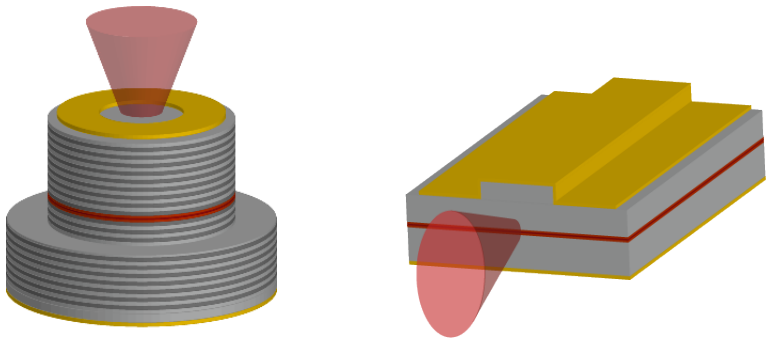

(a) (b)

Figure 2.4: Geometry and optical output direction relative to the orientation of the active region of a) the VCSEL, emitting vertically with a circular beam, and b) the EEL, emitting light along the plane of the layers with an elliptic beam.

divergent beam. The geometry also enables on-wafer testing and fabrication of 2D-arrays. [27]

In a VCSEL, the length of material that provides gain inside the cavity is very short. The radiation from stimulated emission is only amplified during a limited part of a cavity round trip. To increase the stimulated emission rate and achieve lasing, multiple quantum wells (MQW) are introduced in the active region. The QWs provide higher gain for equal carrier density compared to bulk material [27]. The mirrors on either side of the active region also need to be highly reflective so that photons will pass several times through the active region before leaving the laser. The semiconductor distributed Bragg reflector (DBR) relies on reflection and transmission of light at interfaces of two different materials having two different refractive indices, a mirror pair. Each layer, being a quarter wavelength thick, reflects light at the interfaces that add in phase. These mirror pairs can be stacked and designed to provide power reflectance values close to 100%. About 20 mirror pairs are needed to obtain the required minimum reflectivity of 99.8%. The VCSEL structure is almost in its entirety constituted by the two DBRs. This makes the DBR stack important for the performance of the device. Low strain DBR designs can be realized using $Al_xGa_{1-x}As$ compounds, since the lattice constant of GaAs is very close to that of AlAs. [28]

The many passes of a single photon through the active region of the VCSEL lead to a low threshold current. As for any type of semiconductor laser, the performance of a VCSEL is temperature dependent. The emission wavelength is determined by the cavity resonance wavelength rather than the wavelength of the peak of the gain spectrum, as opposed to a Fabry-Perot type of EEL.

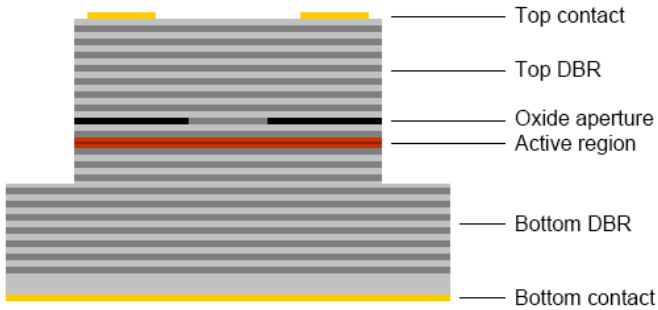

Figure 2.5: Oxide-confined VCSEL.

The gain peak is determined by the material composition and layer thicknesses of the QWs in the active region. The performance of the device depends on the spectral alignment (detuning) between gain peak and cavity resonance, which changes with temperature. [27]

The DBRs confine the light in the longitudinal direction of the VCSEL and an oxide-aperture is used for transverse optical and current confinement, which is illustrated in Figure 2.5. The oxidized layer has a lower refractive index than the non-oxidized layer in the center of the structure. The resulting index-guiding provides transverse optical confinement and determines the number of transverse modes. By reducing the oxide aperture size, the higher order modes can be cut-off and SM behavior can be achieved. The oxide aperture can be formed during fabrication with less complexity than other alternatives for transverse confinement. [27]

A further discussion on VCSEL dynamics and high-speed VCSEL design is presented in the next chapter, Chaper 3.

Chapter 3

High-Speed VCSELs

VCSELs are key components for OIs in data centers. By careful VCSEL design, the OI BW-distance product can be increased. In the OI, the intensity of the VCSEL is directly modulated by current which is repeatedly switched between states, representing logical ones and zeros. For high data rates, the VCSEL must be designed to handle very abrupt transitions.

The dynamic properties of the VCSEL are governed by the close coupling between carrier and photon densities through stimulated emission. The response to an abrupt change in current is that of a second-order system, with the output power of the VCSEL approaching the new level with a certain rise or fall time while undergoing a damped oscillation, referred to as relaxation oscillation. The rise and fall times and the strength and duration of the oscillation are parameters of great importance for data transfer. High-speed modulation requires short rise and fall times, e.g. high modulation BW, and a sufficiently damped modulation response for the oscillation to settle before the next bit slot to avoid excessive timing jitter. This calls for trade-offs in the design.

3.1 VCSEL Dynamics, Speed Limitations and Modal Properties

The following analysis and related equations are derived from [27].

Insight into the dynamics and speed limitations of VCSELs can be gained by considering the SM rate equations, i.e. assuming a single dominant transverse mode:

$$\frac{dN}{dt} = \frac{\eta_i I}{qV_a} - \left(AN + BN^2 + CN^3\right) - v_g GS \tag{3.1}$$

$$\frac{dS_m}{dt} = \Gamma v_g GS - \frac{S}{\tau_p} + \Gamma\beta BN^2 \tag{3.2}$$

where N is the excess carrier density in the active region, η_i the internal quantum efficiency, I the bias current, q the elementary charge, V_a the active region volume, A the Shockley-Read-Hall recombination coefficient , B the radiative recombination coefficient, C the Auger recombination coefficient, v_g is the group velocity, G the active region gain per unit length, S the photon density in the cavity, Γ the longitudinal confinement factor, τ_p the photon lifetime, and β the fraction of the spontaneous emission that goes into the lasing mode.

The SM rate equations are also applicable to the analysis of the dynamics of index guided MM VCSELs with highly overlapping optical fields and uniform carrier and photon densities. Gain compression is accounted for by writing the optical gain as:

$$G = \frac{G_0}{1 + \epsilon S}. \tag{3.3}$$

where G_0 is the unsaturated gain and ϵ is the gain compression factor.

The following small-signal modulation transfer function can be derived from the SM rate equations by assuming small changes of the densities from steady state values:

$$H(f) = \text{const} \cdot \frac{f_r^2}{f_r^2 - f^2 + j\frac{f}{2\pi}\gamma}. \tag{3.4}$$

with

$$f_r \approx \frac{1}{2\pi}\sqrt{\frac{v_g g_0 S}{\tau_p\left(1 + \varepsilon S\right)}}, \tag{3.5}$$

where g_0 is the nominal differential gain (dG_0/dN), and:

$$\gamma \approx K f_r^2 + \gamma_0, \qquad \text{with} \qquad K = 4\pi^2\left[\tau_p + \frac{\varepsilon}{v_g g_0}\right], \tag{3.6}$$

where the resonance frequency f_r and the damping factor γ are characteristic parameters of the modulation response. γ_0 is the damping offset and K is referred to as the K-factor. The relaxation frequency that is limiting the modulation BW is close to the resonance frequency. High differential gain,

high photon density and short photon lifetime give a high resonance frequency. A high differential gain is obtained by strained QWs and proper detuning. The photon density and photon lifetime are largely controlled by the reflectivity of the outcoupling DBR. In order to quantify the rate at which the resonance frequency increases with increasing bias current, the D-factor is introduced:

$$f_r = D \cdot \sqrt{I - I_{th}}, \quad \text{with} \quad D = \frac{1}{2\pi}\sqrt{\frac{\eta_i \Gamma v_g}{qV_a} \cdot g_0}, \tag{3.7}$$

where I is the bias current and I_{th} the threshold current.

The small-signal modulation response can be measured to get an indication of the high-speed performance of the VCSEL. Estimations of the resonance frequency, the damping rate, and the K- and D-factors can then be extracted by a three-parameter fit to the transfer function stated in Equation 3.4, when multiplied with a single pole transfer function to also account for the effects of parasitics (resistances and capacitances). The modulation BW f_{3dB} is defined as the frequency where the response in Equation 3.4 has dropped to half (-3 dB) of its low-frequency value. The modulation BW is limited by either parasitics, thermal effects or damping, or a combination thereof. [29]

Damping flattens the modulation response and increases with photon density, and is also increased by gain compression. Gain compression is due to gain being reduced at high photon densities because of spectral hole burning and hot carrier effects in the gain region. Spectral hole burning is due to carrier depletion at energy levels involved in the stimulated emission process. Below a few GHz, distortion of transitions is dominated by spatial hole burning, while non-linear effects of the relaxation oscillation distort the transitions at higher frequencies. Maximum distortion occurs at the relaxation oscillation frequency and is strongly related to damping. [30]

Thermal effects limit the BW by reducing differential gain and increasing leakage current from the MQW at high internal VCSEL temperatures. Self-heating with current in a VCSEL is typically dominated by resistive heating in the DBRs and internal optical loss due to free-carrier absorption. [31] The main parasitic elements of an oxide-confined VCSEL are the resistances in the DBRs and the capacitance associated with charge stored over the oxide layer. An additional capacitance comes from the capacitance under the bond pad, but this can be made much smaller than the oxide capacitance. [32, 33]

SM and MM VCSELs, with emission spectra shown in Figure 3.1, differ in their dynamic behavior. The narrower spectral width of a SM device improves fiber propagation and enables higher BRs over longer distances. VCSELs can be made SM by reducing the oxide aperture size. The SM device has strong non-linear gain suppression, due to higher photon density in the center of the device and strong lateral carrier diffusion, and therefore the modulation relaxation oscillations are more damped. A small oxide aperture confines current to

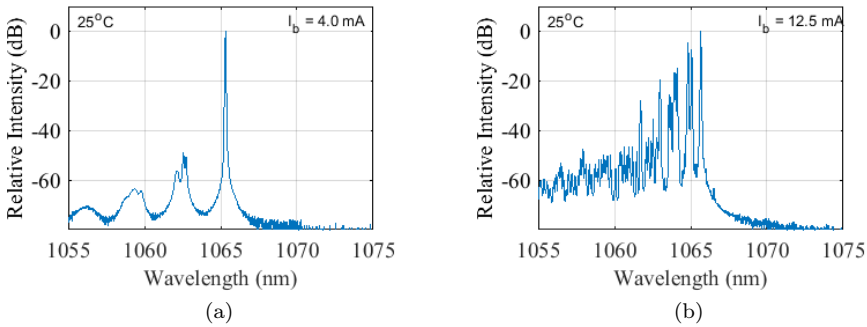

Figure 3.1: Representative spectra for a a) SM VCSEL, and a b) MM VCSEL.

a small volume, which lowers the threshold current but causes increased differential resistance, leading to more self-heating that results in lower maximum output power. The SM VCSEL has a lower beam divergence which improves coupling efficiency to the optical fiber. If the tip of the oxide aperture is placed where the optical field is low, the optical confinement is reduced, the mode size increases, and the beam divergence is reduced [34]. The oxide layer can then be made thicker to reduce capacitance. A tapering of the tip can be used for less diffraction loss. The transverse modes of a MM VCSEL are distinguished by their different spatial intensity distributions and resonance wavelengths. A strongly guided cavity increases the number of supported modes. The modes compete for available carriers in the QWs. The individual intensity distributions of the modes make them overlap differently with carrier density in the QWs and give them different modal gain. The modes also experience different loss due to their different extension in the lateral direction. Modes that overlap less with each other have a higher probability to coexist. At higher currents, thermal lensing will squeeze modes together and increase the number of supported modes. Spatial hole burning locally depletes carriers in the QWs, and when carrier drift and diffusion are not enough to replenish the depletion, other modes may become supported. There are many ways to intentionally change the modal loss or gain and/or use transverse guiding to select lasing modes. Under current modulation, the intensity is distributed unequally between the modes. To avoid signal distortion it is therefore important to collect as much as possible of the light emitted by the different modes of a MM device, while SM devices are less sensitive to spatial filtering. [35–37]

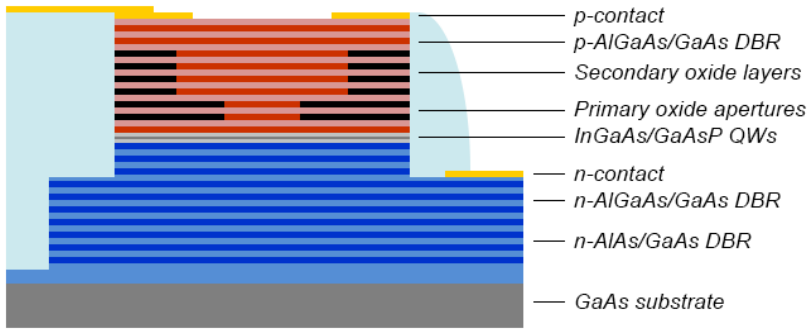

Figure 3.2: Cross sectional view of a 1060 nm oxide-confined GaAs VCSEL structure, showing the top and bottom mesa, contact placement and BCB planarization.

3.2 Design of 1060 nm VCSELs

The VCSELs that are presented in this work (Papers A and B) have been designed for 1060 nm to enable high speed and extended reach, as discussed in Chapter 1, by utilizing the improved fiber properties at longer wavelengths, as discussed in Section 2.1, while maintaining the benefits of the GaAs technology, as discussed in Section 2.2.

There are two 1060 nm high-speed designs, referred to as D1 and D2, derived from our previous 850 nm designs [38] and [39], respectively. In each design, the epitaxial structure is composed of approximately 400 semiconductor layers with varying thickness, composition and doping. These layers mainly form the active region and the surrounding DBRs, including the oxide layers. The device structure, shown in Figure 3.2, is a *p*-side up top-emitting circular double mesa structure encapsulated in benzocyclobutene (BCB). The top mesa defines the size of the oxide apertures and minimizing the diameter of the top mesa and planarizing the structure with BCB helps to reduce capacitance.

In the active region, the very core of the VCSEL, there are three $In_xGa_{1-x}As$ QWs. The strain in the MQW provides high differential gain, which promotes high speed [40, 41]. There are strain-compensating $GaAs_yP_{1-y}$ barriers between the QWs to reduce the net strain of the active region. Devices containing In in the QWs have also been shown to have good reliability [22]. The designs all use a short half-wavelength cavity to maximize the field intensity over the MQW and promote high speed [41]. This is illustrated in Figure 3.3a and 3.3b.

1060 nm VCSELs can achieve higher energy efficiency and temperature stability compared to 850 nm devices. The QWs are deeper, which lowers the leakage currents, especially at higher temperatures. The bandgap is reduced,

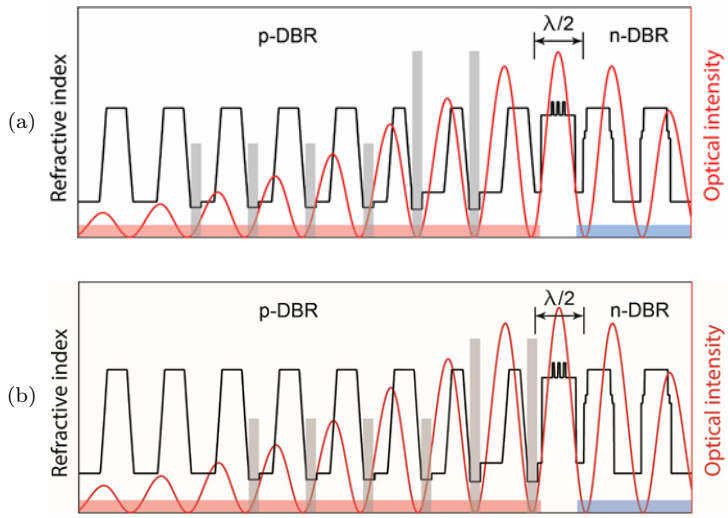

Figure 3.3: Refractive index and optical intensity in the longitudinal direction close to the active region of the VCSEL for Design a) D1, and b) D2. The p- and n-doped DBRs are indicated, as well as the positions of the oxide aperture layers (grey bars).

and it is possible to use lower drive voltages. Since GaAs is non-absorbing at 1060 nm, there is also room for use of more binary compounds throughout the VCSEL structure to decrease thermal impedance. [27, 40]

The DBRs on either side of the active region have graded composition interfaces between the low index $Al_xGa_{1-x}As$ and high index GaAs layers. The refractive index difference must be large between the two mirror pair materials to achieve as high reflectivity as possible. To then avoid abrupt potential discontinuities in the DBRs that add resistance to the current injection in the longitudinal direction, the material composition is graded at the interfaces, using continuous grading in the p-DBR and step-grading in the n-DBR. The electrical conductivity is also improved by modulation doping. High doping levels can have a large impact on optical field loss, since photons are absorbed by free-carrier absorption [31]. Modulation doping is used to keep doping levels low in areas where the optical field intensity is high, thereby minimizing internal optical loss, and still be able to have very thin, highly doped regions close to the interfaces, where the intensity of the optical field is low, to gain the benefits of reducing the effective barrier height. AlAs is used as the low index material in the bottom part of the n-DBR to improve thermal impedance. [28]

The emission wavelength of the VCSEL is determined by the cavity resonance and the wavelength of the gain peak is determined by the material

composition and layer thickness of the QWs. The gain peak shifts with temperature a few times faster than the cavity resonance [32, 42]. The increasing misalignment at high current and temperature leads to a saturation of output power. The gain peak is therefore set at a shorter wavelength than the cavity resonance, 1045 nm compared to 1060 nm. The threshold current is highly dependent on the detuning of the cavity resonance and gain peak. The VCSEL design can be optimized for either low threshold current, high power or temperature independent threshold current and output power.

Transverse optical and current confinement is achieved by two primary oxide apertures positioned on the *p*-side at optical field nodes. Four secondary oxide layers further reduce capacitance over the structure. D1 has oxide layers that are 30 nm thick, while the thinner oxide layers of D2 are 20 nm thick and all placed one mirror pair closer to the active region, see Figure 3.3. Thin oxides placed at field nodes result in weak optical guiding [43]. D2 therefore has lower beam divergence and reduced spectral width, which is beneficial for long distance transmission [34]. With the primary oxide apertures closer to the active region, carrier confinement improves, which facilitates SM operation.

3.3 Fabrication

The fabrication of the 1060 nm VCSELs was performed in a controlled environment, a cleanroom facility, where contamination from environmental pollutants is limited, interfering UV radiation is filtered out, and the air temperature and humidity are stable. Throughout the fabrication, the samples were also thoroughly cleaned with solvents to reduce the effects of surface contamination.

Only standard processing techniques are required and there is no increase in complexity compared to fabrication of 850 nm VCSELs. The process lithography is relatively insensitive to resolution, requiring µm precision, and was achieved solely by UV photolithography.

The epitaxial growth was done by metal-organic chemical vapor deposition (MOCVD) on an undoped GaAs substrate at IQE Europe. Once the material is obtained, it is cleaned and prepared by lithography and an oxide strip (HCl wet etch) for deposition of Ti/Pt/Au *p*-contact rings and alignment marks using electron beam evaporation, see Figure 3.4a. A Si_xN_y cap is deposited by sputtering to protect the GaAs surface in the center of the *p*-contacts, defined by lithography and NF_3 inductively-coupled plasma (ICP) reactive ion etching (RIE), before the top mesa is etched by $SiCl_4$ ICP-RIE, seen in Figure 3.4b. A second layer of Si_xN_y is deposited, this time by plasma-enhanced chemical vapor deposition (PECVD), and removed from the mesa sidewall by NF_3 ICP-RIE after patterning by lithography. Oxide apertures are then formed by subjecting the sample to wet oxidation at high temperature, as in Figure 3.4c. Al-rich DBR layers will oxidize at faster rate with increasing Al-content. The

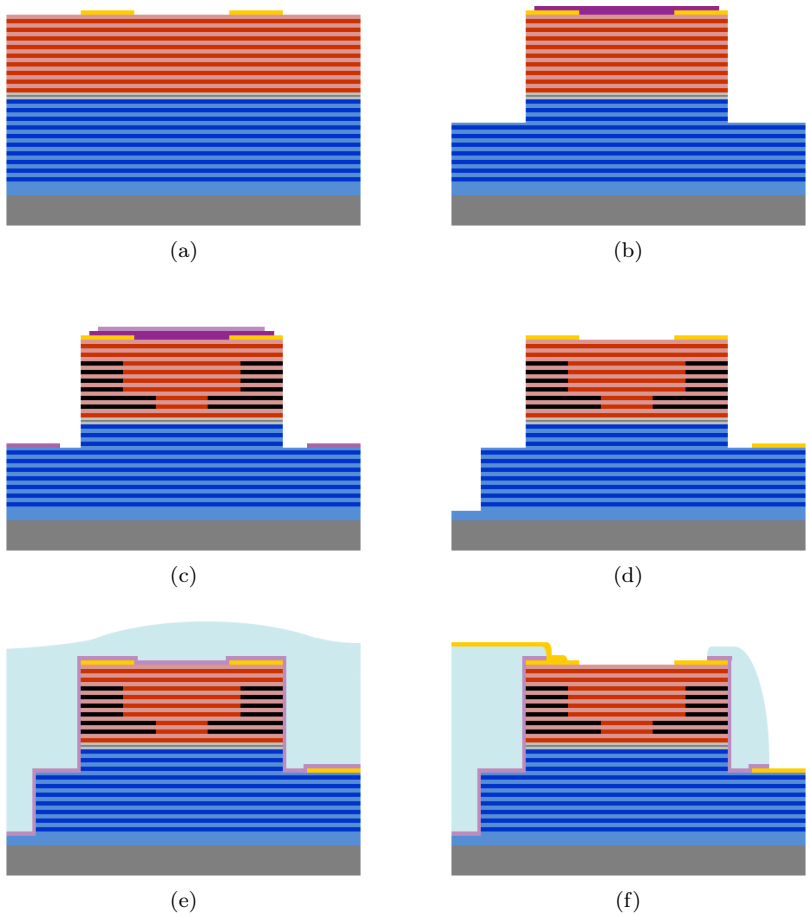

Figure 3.4: The process steps for fabrication of 1060 nm high-speed VCSELs include a) deposition of p-contacts, b) top mesa etching and Si_xN_y deposition, c) oxide aperture formation and Si_xN_y removal, d) deposition of n-contacts and bottom mesa etching, e) Si_xN_y deposition and spin-coating of BCB, and f) BCB planarization, opening of the top mesa surface and contacts, and deposition of contact pads.

oxide aperture sizes are controlled by infrared microscopy and the protective Si_xN_y layers are etched away by NF_3 ICP-RIE.

A fourth lithography step defines the shape of the n-contacts and the surface oxide is again stripped before metal deposition. The electron beam evap-

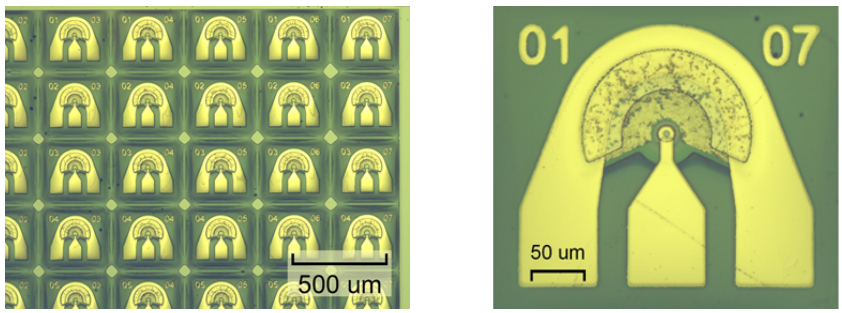

(a) (b)

Figure 3.5: Top view of a) an array of VCSELs, and b) a single fabricated 1060 nm VCSEL.

orated Ni/Ge/Au n-contacts are annealed in a rapid thermal processor (RTP). The annealing temperature is ramped slowly and is kept below the temperature of the previous wet oxidation. Contact anneal can introduce strain in the VCSEL structure, but it improves the ohmic properties of the contacts. The bottom mesa is formed by lithography and $SiCl_4$ ICP-RIE, see Figure 3.4d. Transfer length method (or transmission line model) (TLM) test structures on the wafer can now be used to determine the quality of the contact formation.

Si_xN_y is deposited in a thin layer accross the surface by PECVD. BCB is then spin-coated onto the sample, exposed, developed and hard cured in an oven. Figure 3.4e shows the approximate shape of the thick BCB before planarization begins. Multiple lithography steps with various masks are used to first reduce the peak BCB thickness, then open up for the n-contacts and the p-contacts and finally removing the remaining Si_xN_y at the surface. The BCB has an etch rate similar to that of the resist in O_2/CF_4 ICP-RIE. As BCB planarization is complete, Ti/Au contact pads are sputtered on top, see Figure 3.4f, preceded by lithography and an oxide strip. The final processing fine-tunes the top DBR reflectivity by thinning a GaAs phase tuning layer at the top of the DBR [29] by Ar ion milling.

An array of finished devices is depicted in Figure 3.5a, and a closer top view of the fabricated VCSEL is seen in Figure 3.5b. The large contact pads simplify probing with groung-signal-ground probes. The 15 µm diameter top mesa of the VCSEL is indicated by the p-contact circle in the center of the image.

Chapter 4

Long-Reach VCSEL-Based Optical Interconnects

The need for extended reach OIs has led to developments that build upon the standard 850 nm VCSEL-MMF technology. Short-reach OIs most commonly employ MM VCSELs and high modal BW OM4 MMF [20]. With simple binary modulation and no use of digital signal processing (DSP) to increase capacity, these links have a reach limited to about 100 m at 25-28 Gb/s [44, 45]. Reach is limited by fiber chromatic dispersion and attenuation at high BR. At 850 nm, fiber chromatic dispersion is as high as -85 ps/nm/km, and fiber attenuation exceeds 2 dB/km [17]. If the optical modulation amplitude is large enough, higher order modulation formats can be used to increase the transmission BR. With four-level pulse amplitude modulation (PAM-4), 50-56 Gb/s can be achieved over 100 m OM4 MMF [44, 45]. PAM-4 and other advanced modulation formats can be used together with pre-emphasis, equalization, and forward error correction (FEC). Heavy use of FEC and other forms of DSP is used to mitigate impairments caused by the limited BW and non-linear response of the VCSEL, the fiber modal and chromatic dispersion, and the limited receiver BW. This leads to increased complexity, latency, and power consumption. In addition to improved VCSEL design (with increased modulation BW, reduced parasitics and improved thermal properties), extending reach would benefit from improved fiber performance to enable system implementations with simple modulation formats and a minimum of DSP.

The VCSEL-MMF link reach can be improved by using MMF exhibiting modal-chromatic dispersion compensation properties or SM VCSELs with a narrow spectral width [46]. SMF is an option for very long reach but the transceiver cost is high due to tight alignment tolerances [19]. The fiber performance in terms of chromatic dispersion and attenuation improves at longer

wavelengths [17]. The ideal wavelength is 1310 nm where chromatic dispersion is near zero and attenuation of MMF is only about 0.4 dB/km. However, the GaAs-based VCSEL technology, which is superior to the InP-based in terms of speed, efficiency, manufacturability, and cost-efficiency, can only be extended to about 1100 nm using conventional compound semiconductors without compromising reliability [47]. This has created an interest in GaAs-based VCSELs at wavelengths just below 1100 nm where the fiber chromatic dispersion is -30 ps/nm/km and attenuation is below 1 dB/km [17]. These are large improvements with respect to 850 nm. This justifies the development of GaAs-based 1060 nm SM and MM VCSELs for OIs employing SMF or MMF. When MMF is used, the refractive index profile of the fiber must be optimized to minimize the differential mode delay for high modal BW at the operating wavelength.

4.1 Review of Previous Work

A summary of previously published work on VCSEL-based OIs for extended reach is presented in Paper B, starting with 850 nm VCSEL-MMF links. At 850 nm, 56 Gb/s PAM-4 was enabled over 200 m with modal-chromatic dispersion compensated OM4 fiber using equalization and FEC [48]. SM VCSELs with narrow spectral width have achieved 25 Gb/s on-off keying (OOK)over 1300 m OM4 fiber without equalization or FEC [49], 54 Gb/s OOK over 2200 m OM4 fiber with equalization and FEC [50], 49 Gb/s transmission over 2200 m OM4 fiber using discrete multitone (DMT) modulation and FEC [51], and 135 Gb/s DMT over 550 m OM4 fiber with equalization and FEC [52]. More limited reach extension at high data rates has been demonstrated with MM VCSELs by improving VCSEL parameters such as modulation BW, rise and fall times, and intensity noise, and using techniques such as pre-emphasis, equalization, and advanced modulation formats. This includes 60 Gb/s OOK over 107 m OM3 fiber using equalization (no FEC) [53], 64 Gb/s PAM-4 over 2000 m OM4 fiber using equalization and FEC [54], and 100 (70) Gb/s duobinary PAM-4 over 300 (500) m OM4 fiber with equalization and FEC [55]. In addition, shortwave wavelength division multiplexing with 4 channels (SWDM4) has demonstrated 212 Gb/s (4 x 53 Gb/s PAM-4) and 400 Gb/s (4 x 100 Gb/s PAM-4) over 300 and 105 m of wideband MMF, respectively, both using equalization and FEC [56, 57], and 176 Gb/s (4 x 44 Gb/s OOK) over 100 m OM4 fiber using equalization but no FEC [47].

The first reports on near 1100 nm VCSELs came from NEC. Using strained InGaAs/GaAs QWs with doped barriers for high differential gain and reduced gain compression, and implantation to reduce capacitance, oxide-confined MM VCSELs at 1090 nm with a modulation BW of 20 GHz and transmission capacity of 25 Gb/s OOK were demonstrated in 2006 [58]. With strained InGaAs/GaAsP QWs, the high temperature performance was improved and

25 Gb/s OOK data transmission at 100^{o}C was demonstrated [22]. The oxide aperture was also replaced by a buried-tunnel junction, which allows for current injection through an intra-cavity n-GaAs layer for low resistance [59]. With a BW of 24 GHz, this VCSEL enabled data transmission at 40 Gb/s OOK [60].

Work on 1060 nm VCSELs has been conducted at UC Santa Barbara. Using strained InGaAs/GaAs QWs with doped barriers and multiple oxide apertures for low capacitance, bottom-emitting VCSELs with a BW of 18 GHz and operation at 25 Gb/s OOK [61] were demonstrated. The data rate was extended to 30 Gb/s using pre-emphasis and FEC [62]. However, most of the work on 1060 nm VCSELs has been conducted by Furukawa [63]. Using double intra-cavity contacts and a dielectric top DBR, low-resistance high-efficiency oxide-confined VCSELs with a modulation BW of 20 GHz were demonstrated. This enabled transmission at 25 and 28 Gb/s OOK over 1000 and 500 m of 1060 nm optimized MMF, respectively [25, 64, 65]. With VCSELs from Furukawa, Georgia Tech demonstrated 50 Gb/s PAM-4 transmission over 310 m of wideband MMF using pre-emphasis and FEC [66]. Finally, Hewlett Packard Enterprise have demonstrated 990-1065 nm oxide-confined, bottom emitting, and lens-integrated VCSELs with strain-compensated InGaAs/GaAsP QWs and transmission at 25 Gb/s OOK over 75 m of OM3 fiber [67]. They also recently demonstrated 25 Gb/s OOK and 50 Gb/s PAM-4 transmission over 2000 m of standard SMF using a SM version of the 1065 nm VCSEL [68].

At the somewhat shorter wavelength of 980 nm, where the improvements of fiber chromatic dispersion and attenuation are not as large, very small aperture oxide-confined VCSELs with a modulation BW exceeding 30 GHz were demonstrated recently [69]. With a larger aperture size, data transmission at 50 Gb/s up to 75^{o}C was achieved [70].

In Papers A and B, we present the design and performance of our 1060 nm oxide-confined VCSELs with strain-compensated InGaAs/GaAsP QWs, using OOK and no DSP. At the time of publication, Paper A reported record modulation speed SM VCSELs at 50 Gb/s, measured at room temperature, and 40 Gb/s at 85^{o}C. In Paper B, preliminary data transmission experiments show 25 Gb/s over 1 km 1060 nm optimized MMF. Further improvements are expected by optimizing launch conditions, as described in the following section.

4.2 Launch Conditions and Alignment Tolerances

850 nm VCSEL and MMF links have a relatively relaxed alignment requirement between the VCSEL and the large core (50 µm diameter) fiber. Reflective feedback can be mitigated by aligning the VCSEL output at an angle to the fiber end. Figure 4.1 shows the measured coupling efficiency as a function of misalignment between a 1060 nm MM VCSEL and a MMF. The coupling

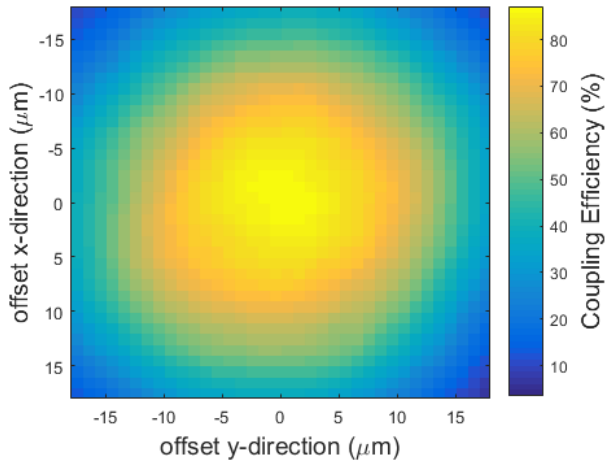

Figure 4.1: Coupling efficiency versus MMVCSEL-MMF alignment offset. A short (1 m) MMF with tilted fiber tip was used to measure the lens coupled power in the fiber from a MM 1060 nm VCSEL with varying offset to the center of the core (position (0,0)).

efficiency is above 70% for up to ±10 µm misalignment with respect to the center of the fiber core. With MM VCSELs, an over-filled launch is frequently used to excite most of the mode groups in the MMF.

SM VCSELs can be used in combination with MMF to reduce the impact of fiber chromatic dispersion that limits the OI transmission speed and distance. The SM VCSEL has a less divergent output beam which improves coupling efficiency. With benefit for longer reach but at the cost of higher required alignment precision, SM VCSELs can also be used to reduce the impact of fiber modal dispersion through selective launch into specific modes groups of the MMF [71]. By matching the size of the Gaussian mode of the SM VCSEL to that of the lowest-order mode in the MMF, only the fundamental mode (or lowest order mode group) will be excited in the fiber.

SMF only supports propagation of the fundamental mode and is therefore free of inter-modal dispersion. However, the smaller core diameter reduces the SM VCSEL-SMF alignment tolerance and thus makes SMF OIs less cost-efficient. [19]

4.3 Future Work

We will continue our work with 1060 nm SM VCSELs and 1060 nm optimized MMF links, by using selective modal launch in transmission experiments. The aim is to investigate what BRs can be achieved with increasing distance, as the effects of attenuation, chromatic dispersion as well as modal dispersion are reduced. There is also an interest in studying the restriction on alignment tolerance, with both radial and angular fiber misalignment, and the sensitivity to optical feedback from external reflections of 1060 nm SM VCSELs.

1060 nm SM VCSELs will also be tested for long reach transmission over 1060 nm SMF. The maximum data rate for different transmission distances is of interest, as is an estimation and comparison of the alignment tolerance to the case of MMF.

The relatively low output power of SM VCSELs can be problematic for the power budget for long-distance transmission. Therefore, it would be of interest to compare the performance of 1060 nm SM VCSELs with and without an integrated mode filter, in terms of resistance, thermal saturation, mode suppression, and dynamics. A low resistance VCSEL with high suppression of higher order modes can be obtained by etching a surface relief centered on top of the top DBR to introduce mode selective loss. A low resistance SM VCSEL also has potential to perform well in PAM-4 transmission over both MMF and SMF, and transmitter pre-emphasis or equalization could be used to further increase capacity.

Chapter 5

Summary of Papers

Paper A

"1060 nm single-mode vertical-cavity surface-emitting laser operating at 50 Gbit/s data rate," *Electronics Letters*, vol. 53, no. 13, pp. 869-871, June 2017.

In this paper we demonstrated that the 1060 nm VCSEL is capable of 50 Gb/s transmission and 40 Gb/s at high temperature. We showed that our design was strongly SM and had low threshold current. In small-signal measurements, the maximum modulation bandwidth was 22 GHz and performance seemed limited by oxide aperture capacitance. These first results showed record speed of near1.1 µm GaAs VCSEs and the energy dissipated during large signal modulation was 100 fJ/bit.

My contribution: I fabricated the VCSELs. The new designs required initial effort to validate the growth and adapt the fabrication process. I performed material tests, determined oxidation rates, etch rates, made simulations, designed new photolithography masks and adjusted all process steps. I performed all measurements, analyzed the results and wrote the paper.

Paper B

"1060 nm VCSELs for long-reach optical interconnects," to be published in *Opt. Fiber Tech. (2018)*, https://doi.org/10.1016/j.yofte.2018.01.001, available online 8 January 2018, (invited paper).

This invited paper, we present the design and performance of our 1060 nm VCSELs, D1 and D2, as well as results from preliminary data transmission experiments using a prototype 1060 nm optimized MMF designed and manufactured by Corning. 25 Gb/s transmission over 1000 m is demonstrated using a single-mode VCSEL and mode-selective launch. This paper also summarizes previous developments and state-of-the-art regarding long-reach optical interconnects.

My contribution: I fabricated the VCSELs, performed all measurements and processed the data. I also designed plots and figures for the paper. Thanks to my hard work in the measurement lab we managed to obtain error-free transmission over 1 km at 25 Gb/s. This required investigations to determine the optimum modulation conditions for different 1060 nm designs and devices and compare their performance.

References

[1] X. Jin, F. Zhang, A. V. Vasilakos, and Z. Liu, "Green data centers: A survey, perspectives, and future directions," *CoRR*, vol. abs/1608.00687, 2016.

[2] S. Mittal, "Power management techniques for data centers: A survey," *CoRR*, vol. abs/1404.6681, 2014.

[3] K. Bilal, S. U. R. Malik, O. Khalid, A. Hameed, E. Alvarez, V. Wijaysekara, R. Irfan, S. Shrestha, D. Dwivedy, M. Ali, U. S. Khan, A. Abbas, N. Jalil, and S. U. Khan, "A taxonomy and survey on green data center networks," *Future Generation Computer Systems*, vol. 36, pp. 189 – 208, 2014. Special Section: Intelligent Big Data Processing Special Section: Behavior Data Security Issues in Network Information Propagation Special Section: Energy-efficiency in Large Distributed Computing Architectures Special Section: eScience Infrastructure and Applications.

[4] L. A. Barroso, J. Clidaras, and U. Hölzle, "The datacenter as a computer: An introduction to the design of warehouse-scale machines, second edition," *Synthesis Lectures on Computer Architecture*, vol. 8, no. 3, pp. 1–154, 2013.

[5] C. Kachris, K. Kanonakis, and I. Tomkos, "Optical interconnection networks in data centers: recent trends and future challenges," *IEEE Communications Magazine*, vol. 51, pp. 39–45, September 2013.

[6] C. Kachris and I. Tomkos, "A survey on optical interconnects for data centers," *IEEE Communications Surveys Tutorials*, vol. 14, pp. 1021–1036, Fourth 2012.

[7] Cisco, "Cisco Global Cloud Index : Forecast and Methodology , 2014-2019," tech. rep., 2016.

[8] L. Wang, F. Zhang, J. A. Aroca, A. V. Vasilakos, K. Zheng, C. Hou, D. Li, and Z. Liu, "Greendcn: A general framework for achieving energy efficiency in data center networks," *IEEE Journal on Selected Areas in Communications*, vol. 32, pp. 4–15, January 2014.

[9] M. Al-Fares, A. Loukissas, and A. Vahdat, "A scalable, commodity data center network architecture," *SIGCOMM Comput. Commun. Rev.*, vol. 38, pp. 63–74, Aug. 2008.

[10] G. Liu, J. Gao, H. Cheng, H. C. Wu, E. Lau, L. Yuan, and C. Krause, "Thunderbolt interconnect; comparing optical and copper approaches," in *2017 IEEE International Symposium on Electromagnetic Compatibility Signal/Power Integrity (EMCSI)*, pp. 305–309, Aug 2017.

[11] H. Cheng, J. Gao, H. C. Wu, G. Liu, E. Lau, L. Yuan, and C. Krause, "Optics vs. copper; from the perspective of thunderbolt 3 interconnect technology," in *2016 China Semiconductor Technology International Conference (CSTIC)*, pp. 1–3, March 2016.

[12] Y. Sun, "Recent advances for high speed short reach optical interconnects for datacom links," in *2017 IEEE CPMT Symposium Japan (ICSJ)*, pp. 63–65, Nov 2017.

[13] A. Ghiasi, "Large data centers interconnect bottlenecks," *Opt. Express*, vol. 23, pp. 2085–2090, Feb 2015.

[14] C. F. Lam, H. Liu, B. Koley, X. Zhao, V. Kamalov, and V. Gill, "Fiber optic communication technologies: What's needed for datacenter network operations," *IEEE Communications Magazine*, vol. 48, pp. 32–39, July 2010.

[15] E. Alliance, "The 2016 Ethernet Roadmap." `http://ethernetalliance.org/roadmap` , accessed 2018-02-19, 2018.

[16] C. Cole, "Beyond 100g client optics," *IEEE Communications Magazine*, vol. 50, pp. s58–s66, February 2012.

[17] M.-J. Li, "Novel optical fibers for data center applications," vol. 9772, 02 2016.

[18] G. Ezeh, "Efficiency of optical fiber communication for dissemination of information within the power system network.," vol. 12, pp. 68–75, 01 2013.

[19] R. E. Freund, C. A. Bunge, N. N. Ledentsov, D. Molin, and C. Caspar, "High-speed transmission in multimode fibers," *Journal of Lightwave Technology*, vol. 28, pp. 569–586, Feb 2010.

[20] M. Freebody, "Lasers evolve to meet the demands of optical communications," vol. 46, pp. 50–53, 02 2012.

[21] N. Bamiedakis, J. Chen, P. Westbergh, J. S. Gustavsson, A. Larsson, R. V. Penty, and I. H. White, "40 gb/s data transmission over a 1-m-long multimode polymer spiral waveguide for board-level optical interconnects," *Journal of Lightwave Technology*, vol. 33, pp. 882–888, Feb 2015.

[22] H. Hatakeyama, T. Anan, T. Akagawa, K. Fukatsu, N. Suzuki, K. Tokutome, and M. Tsuji, "Highly reliable high-speed 1.1-µm-range vcsels with ingaas/gaasp-mqws," *IEEE Journal of Quantum Electronics*, vol. 46, pp. 890–897, June 2010.

[23] S. J. Sweeney, A. F. Phillips, A. R. Adams, E. P. O'Reilly, and P. J. A. Thijs, "The effect of temperature dependent processes on the performance of 1.5-µm compressively strained ingaas(p) mqw semiconductor diode lasers," *IEEE Photonics Technology Letters*, vol. 10, pp. 1076–1078, Aug 1998.

[24] S. Gupta, *Textbook on Optical Fiber Communication and Its Applications*. Prentice-Hall of India, 2004.

[25] T. Kise, T. Suzuki, M. Funabashi, K. Nagashima, and H. Nasu, "The development of the 1060 nm 28 gb/s vcsel and the characteristics of the multi-mode fiber link," *Furukawa Review*, vol. 46, no. Optical Communication, pp. 7–12, 2015.

[26] M.-J. Li, "Mmf for high data rate and short length applications," 03 2014.

[27] L. Coldren and S. Corzine, *Diode Lasers and Photonic Integrated Circuits*. Wiley Series in Microwave and Optical Engineering, John Wiley & Sons, 1995.

[28] S. Adachi, "Lattice thermal resistivity of iii-v compound alloys," *Journal of Applied Physics*, vol. 54, no. 4, pp. 1844–1848, 1983.

[29] P. Westbergh, J. S. Gustavsson, B. Kögel, Å. Haglund, and A. Larsson, "Impact of photon lifetime on high-speed vcsel performance," *IEEE Journal of Selected Topics in Quantum Electronics*, vol. 17, pp. 1603–1613, Nov 2011.

[30] E. P. Haglund, P. Westbergh, J. S. Gustavsson, and A. Larsson, "Impact of damping on high-speed large signal vcsel dynamics," *Journal of Lightwave Technology*, vol. 33, pp. 795–801, Feb 2015.

[31] K. Osamura and Y. Murakami, "Free carrier absorption in n-gaas," *Japanese Journal of Applied Physics*, vol. 11, no. 3, p. 365, 1972.

[32] W. Nakwaski and M. Osiński, "Thermal analysis of etched-well surface-emitting diode lasers," *Microwave and Optical Technology Letters*, vol. 4, no. 12, pp. 541–543, 1991.

[33] P. P. Baveja, B. Kogel, P. Westbergh, J. S. Gustavsson, . Haglund, D. N. Maywar, G. P. Agrawal, and A. Larsson, "Impact of device parameters on thermal performance of high-speed oxide-confined 850-nm vcsels," *IEEE Journal of Quantum Electronics*, vol. 48, pp. 17–26, Jan 2012.

[34] B. Weigl, M. Grabherr, C. Jung, R. Jager, G. Reiner, R. Michalzik, D. Sowada, and K. J. Ebeling, "High-performance oxide-confined gaas vcsels," *IEEE Journal of Selected Topics in Quantum Electronics*, vol. 3, pp. 409–415, Apr 1997.

[35] Y. Satuby and M. Orenstein, "Mode-coupling effects on the small-signal modulation of multitransverse-mode vertical-cavity semiconductor lasers," *IEEE Journal of Quantum Electronics*, vol. 35, pp. 944–954, Jun 1999.

[36] J. S. Gustavsson, J. Bengtsson, and A. Larsson, "Modal dynamics and noise of vertical-cavity surface-emitting lasers," in *Numerical Simulation of Optoelectronic Devices, 2004. NUSOD '04. Proceedings of the 4th International Conference on*, pp. 53–56, Aug 2004.

[37] J. S. Gustavsson, J. A. Vukusic, J. Bengtsson, and A. Larsson, "A comprehensive model for the modal dynamics of vertical-cavity surface-emitting lasers," *IEEE Journal of Quantum Electronics*, vol. 38, pp. 203–212, Feb 2002.

[38] P. Westbergh, R. Safaisini, E. Haglund, J. S. Gustavsson, A. Larsson, and A. Joel, "High-speed oxide confined 850-nm vcsels operating error-free at 47 gbit/s at room temperature and 40 gbit/s at 85^{o}c," in *2013 Conference on Lasers Electro-Optics Europe International Quantum Electronics Conference CLEO EUROPE/IQEC*, pp. 1–1, May 2013.

[39] E. Haglund, P. Westbergh, J. S. Gustavsson, E. P. Haglund, and A. Larsson, "High-speed vcsels with strong confinement of optical fields and carriers," *Journal of Lightwave Technology*, vol. 34, pp. 269–277, Jan 2016.

[40] R. Nagarajan, M. Ishikawa, T. Fukushima, R. S. Geels, and J. E. Bowers, "High speed quantum-well lasers and carrier transport effects," *IEEE Journal of Quantum Electronics*, vol. 28, pp. 1990–2008, Oct 1992.

[41] S. B. Healy, E. P. O'Reilly, J. S. Gustavsson, P. Westbergh, . Haglund, A. Larsson, and A. Joel, "Active region design for high-speed 850-nm vcsels," *IEEE Journal of Quantum Electronics*, vol. 46, pp. 506–512, April 2010.

[42] A. Mutig, G. Fiol, K. Potschke, P. Moser, D. Arsenijevic, V. A. Shchukin, N. Ledentsov, S. S. Mikhrin, I. L. Krestnikov, D. A. Livshits, A. Kovsh, F. Hopfer, and D. Bimberg, "Temperature-dependent small-signal analysis of high-speed high-temperature stable 980-nm vcsels," vol. 15, pp. 679 – 686, 07 2009.

[43] R. L. Naone, E. R. Hegblom, and L. A. Coldrenz, "Tapered-apertures for high-efficiency miniature vcsels," in *1999 Digest of the LEOS Summer Topical Meetings: Nanostructures and Quantum Dots/WDM Components/VCSELs and Microcavaties/RF Photonics for CATV and HFC Systems (Cat. No.99TH8455)*, pp. III17–III18, July 1999.

[44] J. A. Tatum, D. Gazula, L. A. Graham, J. K. Guenter, R. H. Johnson, J. King, C. Kocot, G. D. Landry, I. Lyubomirsky, A. N. MacInnes, E. M. Shaw, K. Balemarthy, R. Shubochkin, D. Vaidya, M. Yan, and F. Tang, "Vcsel-based interconnects for current and future data centers," *Journal of Lightwave Technology*, vol. 33, pp. 727–732, Feb 2015.

[45] D. Mahgerefteh, C. Thompson, C. Cole, G. Denoyer, T. Nguyen, I. Lyubomirsky, C. Kocot, and J. Tatum, "Techno-economic comparison of silicon photonics and multimode vcsels," *Journal of Lightwave Technology*, vol. 34, pp. 233–242, Jan 2016.

[46] L. Qiu, E. J. Lawrence, B. Ayres, M. Schumacher, A. Amezcua, D. Molin, and G. Kuyt, "40gbase-sr4 frame error rate test of chromatic dispersion compensating mmf," in *2013 Optical Fiber Communication Conference and Exposition and the National Fiber Optic Engineers Conference (OFC/NFOEC)*, pp. 1–3, March 2013.

[47] T. N. Huynh, F. Doany, D. M. Kuchta, D. Gazula, E. Shaw, J. O'Daniel, and J. Tatum, "4 x 50gb/s nrz shortwave-wavelength division multiplexing vcsel link over 50m multimode fiber," in *2017 Optical Fiber Communications Conference and Exhibition (OFC)*, pp. 1–3, March 2017.

[48] J. M. Castro, R. Pimpinella, B. Kose, P. Huang, B. Lane, K. Szczerba, P. Westbergh, T. Lengyel, J. S. Gustavsson, A. Larsson, and P. A. Andrekson, "Investigation of 60 gb/s 4-pam using an 850 nm vcsel and multimode fiber," *Journal of Lightwave Technology*, vol. 34, pp. 3825–3836, Aug 2016.

[49] R. Safaisini, E. Haglund, P. Westbergh, J. S. Gustavsson, and A. Larsson, "20 gbit/s data transmission over 2 km multimode fibre using 850 nm mode filter vcsel," *Electronics Letters*, vol. 50, pp. 40–42, January 2014.

[50] G. Stepniak, J. R. Kropp, N. N. Ledentsov, V. A. Shchukin, N. Ledentsov, G. Schaefer, and J. P. Turkiewicz, "54 gbps ook transmission using single mode vcsel up to 1 km om4 mmf," in *2016 Optical Fiber Communications Conference and Exhibition (OFC)*, pp. 1–3, March 2016.

[51] I. C. Lu, C. C. Wei, H. Y. Chen, K. Z. Chen, C. H. Huang, K. L. Chi, J. W. Shi, F. I. Lai, D. H. Hsieh, H. C. Kuo, W. Lin, S. W. Chiu, and J. Chen, "Very high bit-rate distance product using high-power single-mode 850-nm vcsel with discrete multitone modulation formats through om4 multimode fiber," *IEEE Journal of Selected Topics in Quantum Electronics*, vol. 21, pp. 444–452, Nov 2015.

[52] C. Kottke, C. Caspar, V. Jungnickel, R. Freund, M. Agustin, and N. N. Ledentsov, "High speed 160 gb/s dmt vcsel transmission using pre-equalization," in *2017 Optical Fiber Communications Conference and Exhibition (OFC)*, pp. 1–3, March 2017.

[53] D. Kuchta, A. V. Rylyakov, C. L. Schow, J. Proesel, C. Baks, P. Westbergh, J. S. Gustavsson, and A. Larsson, "64gb/s transmission over 57m mmf using an nrz modulated 850nm vcsel," in *Optical Fiber Communication Conference*, p. Th3C.2, Optical Society of America, 2014.

[54] J. J. Liu, K. L. Chi, C. C. Wei, T. C. Lin, C. Y. Chuang, X. N. Chen, J. W. Shi, and J. Chen, "High bit-rate distance product of 128 gbps.km 4-pam transmission over 2-km om4 fiber using an 850-nm vcsel and a volterra nonlinear equalizer," in *2017 Optical Fiber Communications Conference and Exhibition (OFC)*, pp. 1–3, March 2017.

[55] T. Zuo, L. Zhang, J. Zhou, Q. Zhang, E. Zhou, and G. N. Liu, "Single lane 150-gb/s, 100-gb/s and 70-gb/s 4-pam transmission over 100-m, 300-m and 500-m mmf using 25-g class 850nm vcsel," in *ECOC 2016; 42nd European Conference on Optical Communication*, pp. 1–3, Sept 2016.

[56] F. Chang, Y. Sun, R. Lingle, Y. Zhang, P. Cai, M. Huang, D. Pan, T. Gray, S. Bhoja, S. Nelson, and J. Tatum, "First demonstration of pam4 transmissions for record reach and high-capacity swdm links over mmf using 40g/100g pam4 ic chipset with real-time dsp," in *2017 Optical Fiber Communications Conference and Exhibition (OFC)*, pp. 1–3, March 2017.

[57] J. Lavrencik, S. Varughese, V. A. Thomas, G. Landry, Y. Sun, R. Shubochkin, K. Balemarthy, J. Tatum, and S. E. Ralph, "4λ x 100gbps vcsel pam-4 transmission over 105m of wide band multimode fiber," in *Optical Fiber Communication Conference*, p. Tu2B.6, Optical Society of America, 2017.

[58] N. Suzuki, H. Hatakeyama, K. Fukatsu, T. Anan, K. Yashiki, and M. Tsuji, "25 gbit/s operation of ingaas-based vcsels," *Electronics Letters*, vol. 42, pp. 975–976(1), August 2006.

[59] K. Yashiki, N. Suzuki, K. Fukatsu, T. Anan, H. Hatakeyama, and M. Tsuji, "1.1-µm-range high-speed tunnel junction vertical-cavity surface-emitting lasers," *IEEE Photonics Technology Letters*, vol. 19, pp. 1883–1885, Dec 2007.

[60] N. Suzuki, T. Anan, H. Hatakeyama, K. Fukatsu, K. Yashiki, K. Tokutome, T. Akagawa, and M. Tsuji, "High speed 1.1-Îijm-range ingaas-based vcsels," vol. 92-C, pp. 942–950, 07 2009.

[61] Y. Zheng, C. H. Lin, A. V. Barve, and L. A. Coldren, "P-type δ-doping of highly-strained vcsels for 25 gbps operation," in *IEEE Photonics Conference 2012*, pp. 131–132, Sept 2012.

[62] A. Tatarczak, Y. Zheng, G. A. Rodes, J. Estaran, C. H. Lin, A. V. Barve, R. HonorÃľ, N. Larsen, L. A. Coldren, and I. T. Monroy, "30 gbps bottom-emitting 1060 nm vcsel," in *2014 The European Conference on Optical Communication (ECOC)*, pp. 1–3, Sept 2014.

[63] T. Suzuki, M. Funabashi, H. Shimizu, K. Nagashima, S. Kamiya, and A. Kasukawa, "1060nm 28-gbps vcsel developed at furukawa," vol. 9001, 01 2014.

[64] J. B. HÃľroux, T. Kise, M. Funabashi, T. Aoki, C. L. Schow, A. V. Rylyakov, and S. Nakagawa, "Energy-efficient 1060-nm optical link operating up to 28 gb/s," *Journal of Lightwave Technology*, vol. 33, pp. 733–740, Feb 2015.

[65] K. Nagashima, T. Kise, Y. Ishikawa, and H. Nasu, "A record 1-km mmf nrz 25.78-gb/s error-free link using a 1060-nm dic vcsel," *IEEE Photonics Technology Letters*, vol. 28, pp. 418–420, Feb 2016.

[66] S. K. Pavan, J. Lavrencik, R. Shubochkin, Y. Sun, J. Kim, D. Vaidya, R. Lingle, T. Kise, and S. E. Ralph, "50gbit/s pam-4 mmf transmission using 1060nm vcsels with reach beyond 200m," in *OFC 2014*, pp. 1–3, March 2014.

[67] M. Tan, P. Rosenberg, W. Sorin, S. Mathai, G. Panotopoulos, G. Rankin, and J. Straznicky, "Progress towards low cost tbps optical engines," in *2015 IEEE CPMT Symposium Japan (ICSJ)*, pp. 9–11, Nov 2015.

[68] M. R. Tan, P. Rosenberg, W. V. Sorin, S. Mathai, G. Panotopoulos, and G. Rankin, "Universal photonic interconnect for data centers," 01 2017.

[69] R. Rosales, M. Zorn, and J. A. Lott, "30-ghz small-signal modulation bandwidth with directly current-modulated 980-nm oxide-aperture vcsels," 10 2017.

[70] G. Larisch, P. Moser, J. A. Lott, and D. Bimberg, "Large bandwidth, small current density, and temperature stable 980-nm vcsels," *IEEE Journal of Quantum Electronics*, vol. 53, pp. 1–8, Dec 2017.

[71] L. Raddatz, I. H. White, D. G. Cunningham, and M. C. Nowell, "An experimental and theoretical study of the offset launch technique for the enhancement of the bandwidth of multimode fiber links," *Journal of Lightwave Technology*, vol. 16, pp. 324–331, Mar 1998.